Journal of Hazardous Materials 203–204 (2012) 264–273

Contents lists available at SciVerse ScienceDirect

Journal of Hazardous Materials

journal homepage: www.elsevier.com/locate/jhazmat

Modification of red mud by acid treatment and its application for CO removal

Snigdha Sushil, Vidya S. Batra *

Centre for Energy and Environment, TERI University, 10 Institutional Area, Vasant Kunj, New Delhi 110070, India

ARTICLE INFO

Article history:
Received 10 August 2011
Received in revised form
25 November 2011
Accepted 5 December 2011
Available online 13 December 2011

Keywords:
Carbon monoxide
Activated red mud
Hydroxylated iron oxide
Oxidation

ABSTRACT

Activated red mud (ARM) samples were tested for carbon monoxide (CO) oxidation in the temperature range of 100–500 °C. Conversion of >90% was obtained for temperatures above 400 °C for all samples. In order to study the effect of hydroxylated phases of iron oxide in red mud on the removal of CO, 'as-received' red mud (RM) and acid digested and re-precipitated red mud (TRM) were also tested under similar conditions. It was found that TRM was more effective in removal of CO with the 50% conversion temperature (*T*50) 80 °C lower than the ARM samples. The samples before and after reaction were characterized by inductively coupled plasma-optical emission spectroscopy (ICP-OES), BET N_2 adsorption, X-ray diffraction (XRD), Fourier transform infrared spectroscopy (FTIR), electron microscopy (SEM and TEM) and temperature programmed reduction (TPR). It was observed that TRM had iron in an amorphous form which then converted to iron oxide after heating. The higher activity of TRM was due to its higher surface area and presence of hydroxylated phase of iron oxide.

1. Introduction

CO is a highly toxic gas and its removal from the exhaust gases is essential. Catalytic oxidation is a commonly used method for CO removal. Precious metals (e.g., Au, Pt and Pd) have been found to be quite effective for this purpose [1–3]. However their price, low stability against poisons like Cl^- and availability is a limiting factor. Transition metals and metal oxides on various supports like TiO_2, Al_2O_3, ZnO, Co_3O_4, MnO_2, MgO, Fe_2O_3, Zr_2O_3 are also quite well known for CO oxidation [4–7]. They are cheaper and readily available; however they are less active than the precious metals. The activity and stability of the metal oxides can be increased by dispersing them on a catalyst support [8]. The ease with which a metal oxide (MO) loses its oxygen atom, affects its catalytic activity towards carbon monoxide oxidation to a large extent. The CO oxidation activity for different metal oxides as reported by Shelef et al. [9] was in the following order: Co_3O_4, $CuCr_2O_4 > Cu_2O > Fe_2O_3 > MnO > NiO > Cr_2O_3 > V_2O_5$.

Iron oxide is one of the readily available catalysts for CO oxidation. It shows dual function as a catalyst, in being able to carry out oxidation both in the presence and absence of oxygen. In absence of oxygen it can lose the oxygen bound to its lattice thereby causing direct oxidation and simultaneous reduction of iron oxide. The reduced forms of iron oxide and iron catalyze the disproportionation reaction of carbon monoxide leading to the formation of C and CO_2 [10].

Mondal et al. [11] found that the temperature range of 725–900 °C is favorable for the oxidation of CO to CO_2 over iron oxide in the absence of oxygen. Imai et al. [12] synthesized α-Fe_2O_3 (hematite) by dehydration of goethite at 330 °C, without sintering agents and with low amounts of phosphorous and silica. They observed 99% CO conversion at 300 °C in absence of oxygen.

Red mud, an aluminum industry waste, contains a mixture of many metal oxides, 30–60% of which constitutes Fe_2O_3; in addition, other constituents like TiO_2, Al_2O_3, SiO_2 and traces of V_2O_5 are also present [13,14]. It possesses high surface area, sintering resistance, resistance to poisoning and is available at practically no cost. Given the high volume of red mud generation, many management options and utilization options have been examined which are summarized in recent reviews [15,16]. Few studies have been carried out for using red mud as catalyst for decomposition of methane [17,18], methane combustion [19], VOC (volatile organic compounds) oxidation [20], sulphur dioxide reduction [21], nitric oxide reduction [22], etc.

In the present study, as-received red mud and modified red mud have been investigated for the removal of CO. Studies such as Lin et al. [23] and Li et al.,[10] have investigated the removal of CO on iron oxide and have reported that the presence of hydroxylated group of iron oxide leads to a higher activity. Lin et al. [23] used iron oxide prepared from precipitation method using different solutions of aqueous iron salts while Li et al. [10] used a commercial free flowing power NANOCAT® from Mach, FeOOH and α-Fe_2O_3. Since iron oxide is the main catalytic component in red mud and since in activated red mud (ARM) all or most of the iron is expected to

* Corresponding author at: TERI/TERI University, Darbari Seth Block, Lodhi Road, New Delhi 110003, India. Fax: +90 11 24682144.
E-mail address: vidyasb@teri.res.in (V.S. Batra).

0304-3894/$ – see front matter © 2011 Elsevier B.V. All rights reserved.
doi:10.1016/j.jhazmat.2011.12.007

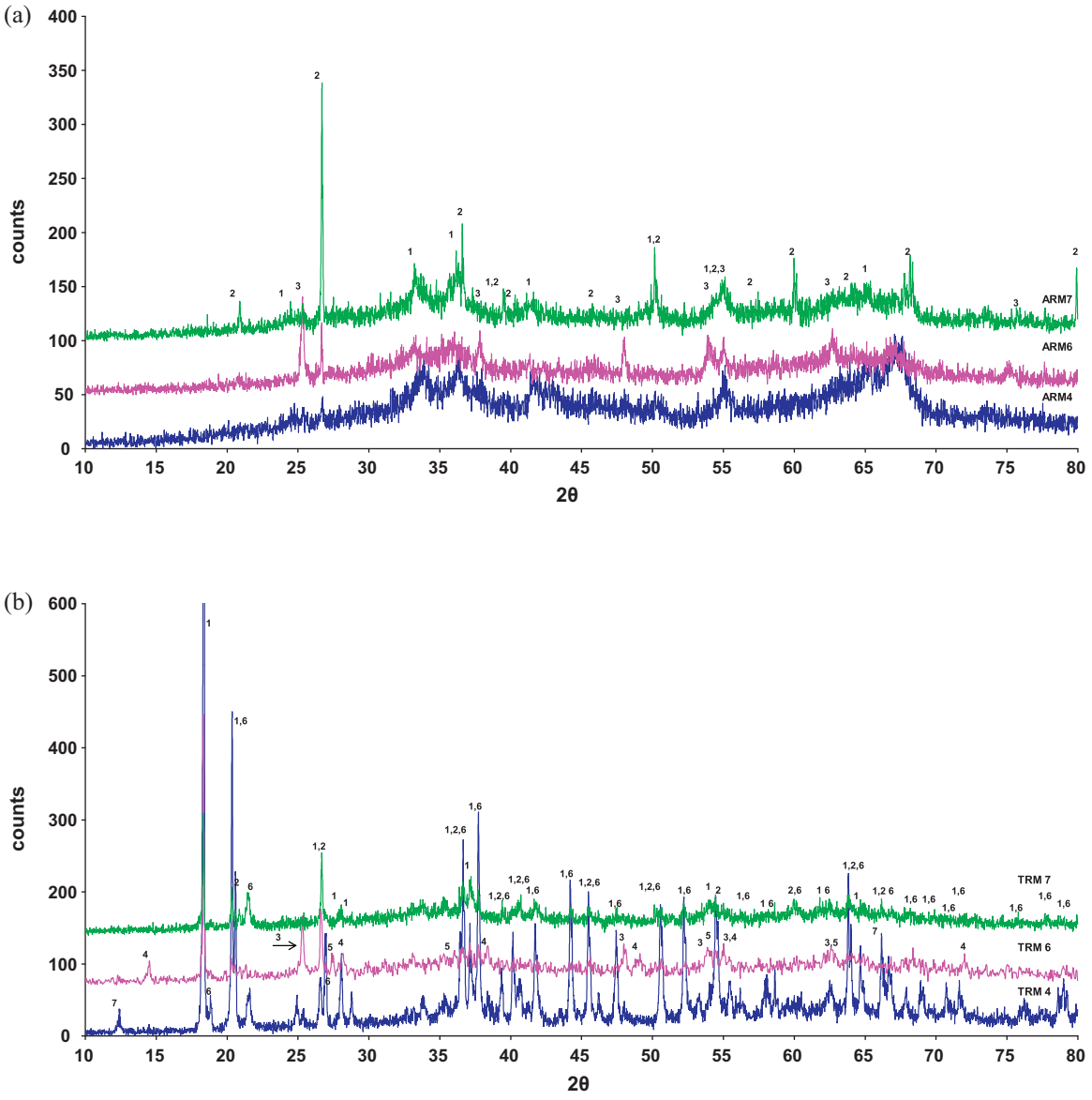

Fig. 1. (a) XRD pattern of ARM: 1, hematite (Fe_2O_3); 2, quartz (SiO_2); 3, anatase (TiO_2). (b) XRD pattern of acid treated red mud: 1, gibbsite ($Al(OH)_3$); 2, quartz (SiO_2); 3, anatase (TiO_2); 4, boehmite (AlO(OH)); 5, titania (TiO_2); 6, bayerite ($Al(OH)_3$); 7, aluminum silicate ($Al_xSi_yO_z$).

be present in the oxide form, we attempted to see the effect of presence of hydroxylated phases in the as-received (RM) and acid treated red mud (TRM) for CO removal and compared it to ARM. The results obtained for red mud samples here were compared with the results obtained for commercial iron oxide.

2. Experimental

2.1. Materials

Red mud (RM) samples were collected from aluminum plants located at different sites in India. RM4 and RM7 were collected from a site in Tamil Nadu with a separation of two years while RM6 tailings were collected from a site in Jharkhand. The samples were dried, ground and sieved to a size of <150 μm. These samples were then characterized using various techniques. The reaction studies were carried out without any pretreatments.

For red mud activation, 10 g of dried and sieved red mud was taken and 190 ml distilled water was added to it. After stirring for 5 min on a magnetic stirrer, 20 ml of 37% HCl (Fluka) was added. The sample was kept for digestion at 80 °C till the time only white residue most likely from undissolved silica and titania was left at the bottom of the digester. The digested sample was then precipitated by adding aqueous ammonia drop-wise and simultaneous stirring till a pH of 8 was reached. The resulting precipitate was centrifuged and washed with warm distilled water to remove residual chlorine. The removal of Cl^- was confirmed by the $AgNO_3$ test. A small amount of Cl^- ion was detected even after several washings. The separated precipitate was kept for drying at 110 °C in the oven for 12 h and was later calcined in static air at 500 °C for 2 h in a muffle furnace. The prepared samples were termed as ARM.

In case of simple acid treatment the procedure was identical to the activation method up to the digestion and precipitation of the sample. From this point the treatment of the sample was different. The precipitate after washing was dried at 120 °C for 24 h in order to preserve the FeOOH group. The prepared samples were termed as TRM.

Commercial Fe_2O_3 was purchased from Qualigens (purity 90%), India and was used without further treatment.

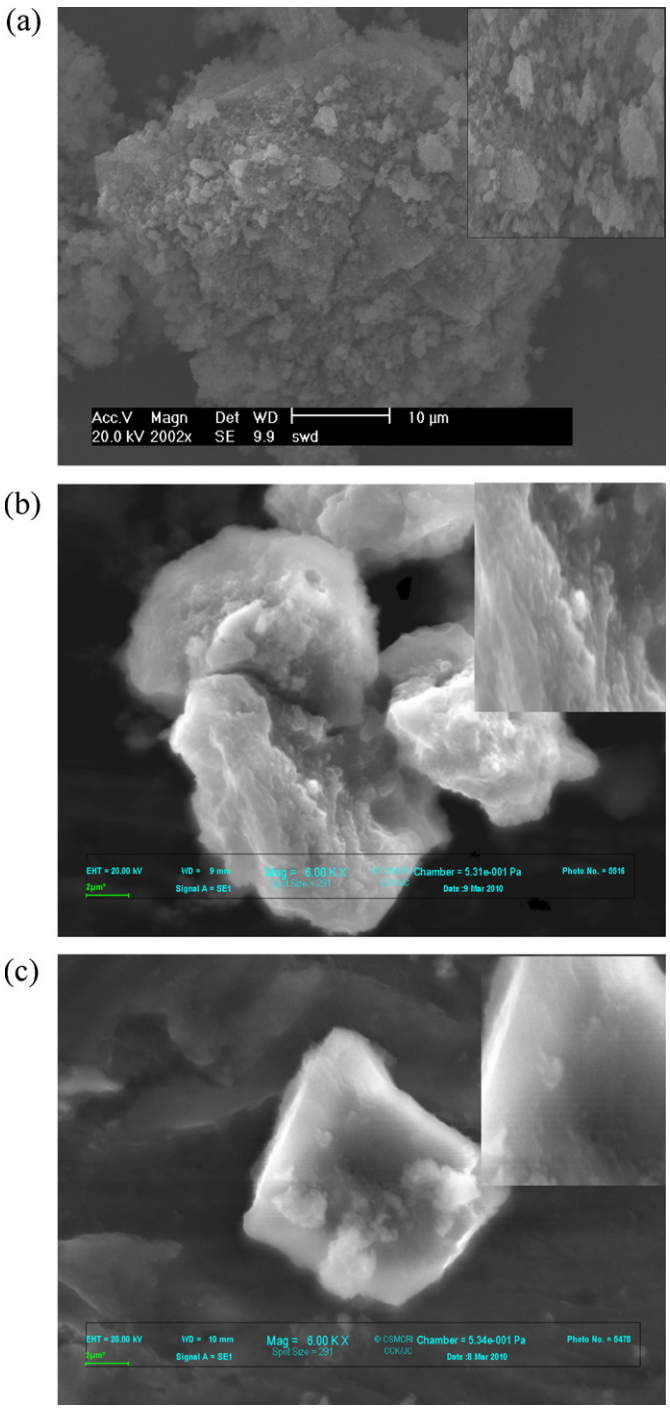

Fig. 2. SEM image for (a) RM7 1000× magnification, (b) ARM7 6000× magnification and (c) TRM7 6000× magnification (inset picture shows enlarged view of a portion of the image).

2.2. Catalyst characterization

The composition of as-received RM was analyzed using ICP-OES. ICP-OES was performed using a Varian ICP Vista MPX model ICPAES radial. Samples were investigated as known masses of fine powders dissolved in mixed acids. Any insoluble portions were given fusion treatment with suitable fluxes and the melt from the fusion treatment was dissolved in dilute acid and mixed with main solution for analysis. Simultaneous analysis against known standards was performed.

BET surface area and total pore volume was measured with SMART Instrument model 92/93 using N_2 adsorption at liquid nitrogen temperature (−196 °C).

The phases present in the samples were determined by X-ray diffraction on X'Pert MPD diffractometer with monochromatic Cu Kα radiations (45 kV, 40 mA). The diffraction angle was swept from 5° to 80° with a step size of 0.02° and step time of 1.0 s. Identification of phases was accomplished by comparison with internationally recognized JCPDS reference patterns.

SEM analysis was conducted on Leo 1430 VP. For preparation of the specimens a small amount of red mud was placed on a two-sided sticky tape resting on an aluminum holder and observed at different magnifications. TEM analysis was done using JEOL, JEM 2100.

The FTIR analysis was done on Spectrum GX from PerkinElmer. The sample pellets were prepared using KBr crystals. The spectra were recorded in the range of 400–4000 cm^{-1} with an instrument resolution of 4 cm^{-1}.

The TPR measurements were carried out on Micromeritics instrument, ChemiSoft TPx V1.02. Prior to the TPR, 100 mg of sample was pretreated at 185 °C in high purity helium gas at the rate of 25 ml min^{-1} for 1 h. The sample was cooled to room temperature before reducing the sample with 5% H_2/Ar at the rate of 25 ml min^{-1}. The TPR was carried out from room temperature to 800 °C at the rate of 10 °C min^{-1}.

2.3. Reaction studies

The catalytic activity of the samples was determined in an electrically heated quartz tube-fixed bed reactor having an internal diameter of 1.8 cm. The catalyst was placed centrally in the reactor supported between quartz wool plug and a porous quartz disc. The temperatures were measured at two points, one just outside the reactor and the second directly in the catalyst bed. A K-type thermocouple was employed for the purpose.

A feed gas mixture of 1% CO, 6% O_2 and balance N_2 was used for the analysis. A flow rate of 50 ml min^{-1} was employed giving a GHSV of 6000 h^{-1}. The product gas mixture was analyzed in a Nucon 5700 GC fitted with an FID with methanizer and carbosphere column of 30 m length and 0.32 mm O.D.

CO oxidation was performed while heating the reactor in temperature ramp from 100 to 500 °C at 30 °C min^{-1}. The conversion was recorded as a function of temperature. The conversion was calculated as follows:

$$\text{CO conversion}\,[\%] = \left\{\frac{(C_o - C)}{C_o}\right\} \times 100$$

where C_o = CO concentration in inlet gas C = CO concentration in outlet gas.

The samples of the outlet gas were taken and analyzed every 10 min. Background experiments were performed using an empty reactor tube containing quartz wool plug only. It was observed that below 600 °C there was negligible contribution of the reactor/temperature on CO oxidation.

3. Results and discussions

3.1. Materials characterization

The compositions of the various as-received RM samples have been reported [17]. Fe_2O_3 is the major constituent in all red mud samples along with SiO_2, Al_2O_3 and TiO_2. Fe_2O_3 content in the range 36–42 wt% was obtained in the as-received red mud. Activation increased the content by 20–30%. Oxides of sodium and calcium are also present in small amounts. RM7 has the highest amount of Na_2O while RM6 has the highest amount of TiO_2. The

Table 1
Surface area of pre-reaction samples.

S. no.	Sample code	Pre reaction surface area ($m^2\ g^{-1}$)
1	RM4	12.37
2	RM6	10.12
3	RM7	11.55
4	Fe_2O_3	5.97
5	TRM4	64.51
6	TRM6	159.75
7	TRM7	219.45
8	ARM4	144.48
9	ARM6	121.68
10	ARM7	151.86

loss on ignition (LOI) of RM6 is low indicating the presence of lower amount of carbonates and oxy/hydroxides compared to RM4 and RM7. CHN analysis of the starting red mud samples showed carbon content of 0.7–1.7 wt% [18].

The specific surface area of the samples of ARM, TRM, RM and Fe_2O_3 is provided in Table 1. The initial surface area of the red mud samples is found to be similar. Fe_2O_3 was found to have a low surface area of 5.97 $m^2\ g^{-1}$.The surface area of both ARM and TRM was found to be higher than the as-received RM. The acid treatment leads to removal of sodium ions and compounds [24,25]. Further it causes dispersion of dissolved metal oxides as hydroxides which leads to formation of pores thereby increasing the surface area [24]. In the activated samples, dehydration during heat treatment also contributes to formation of pores.

From the XRD analysis reported previously [17], as-received RM is found to be a complex mixture of phases mainly comprised of hematite (Fe_2O_3), goethite (FeOOH), gibbsite ($Al(OH)_3$), quartz (SiO_2) and mixed silicates. Ti is present in the form of anatase (TiO_2) in RM6. Fig. 1 (a and b) shows the XRD pattern of ARM and TRM samples. The main phases in ARM are hematite (Fe_2O_3) and quartz (SiO_2) while in TRM the main phases are gibbsite ($Al(OH)_3$), quartz (SiO_2), anatase (TiO_2), boehmite (AlO(OH)), titania (TiO_2), bayerite ($Al(OH)_3$) and aluminum silicate ($Al_xSi_yO_z$). The iron hydroxide is converted to hematite during the heating step of the ARM samples. Fe compound peaks are not observed in TRM and are presumed to be in amorphous form. Lin et al. [23] also obtained amorphous iron oxide under certain preparation conditions; the one with high surface area was very active for CO oxidation.

The SEM images of ARM and TRM when compared to the images of RM, show a smoother surface and the removal of small particles on the surface of red mud can be observed [24] (Fig. 2). TEM images show that ARM and RM have a mixture of crystalline and amorphous phases while TRM is mostly amorphous as also observed in XRD analysis (Fig. 3).

The FTIR spectra of red mud (RM7) activated red mud (ARM7) and acid treated red mud (TRM7) are shown in Fig. 4. Due to the complexity of the sample the peaks were clear only at a higher resolution. The peaks at 3158 cm^{-1}, 3417.4 cm^{-1} and 3524.9 cm^{-1} in RM7, ARM7 and TRM7 respectively correspond to the OH stretching vibration in the samples [26]. The intensity of the OH vibration band was found to be lower in TRM7 and ARM7 as compared to RM7. Vibrations relating to goethite were observed in TRM7 at 970.4 cm^{-1} and close to 800 cm^{-1}, these were not seen in case of ARM7. The intensity of the goethite peaks in TRM was low due to its low crystallinity. The other RM, ARM and TRM samples showed a similar trend.

Stretching vibrations of Fe—O bands of hematite structure could be seen in the RM7 sample at 579 cm^{-1} and 1642 cm^{-1} [27]. In addition vibrations relating to goethite could be observed at 808 cm^{-1} and 989 cm^{-1} [28]. The Fe–O bands could also be observed in AMR7 at 569.4 cm^{-1} and 1633.1 cm^{-1} and in TRM7 at 595.9 cm^{-1} and

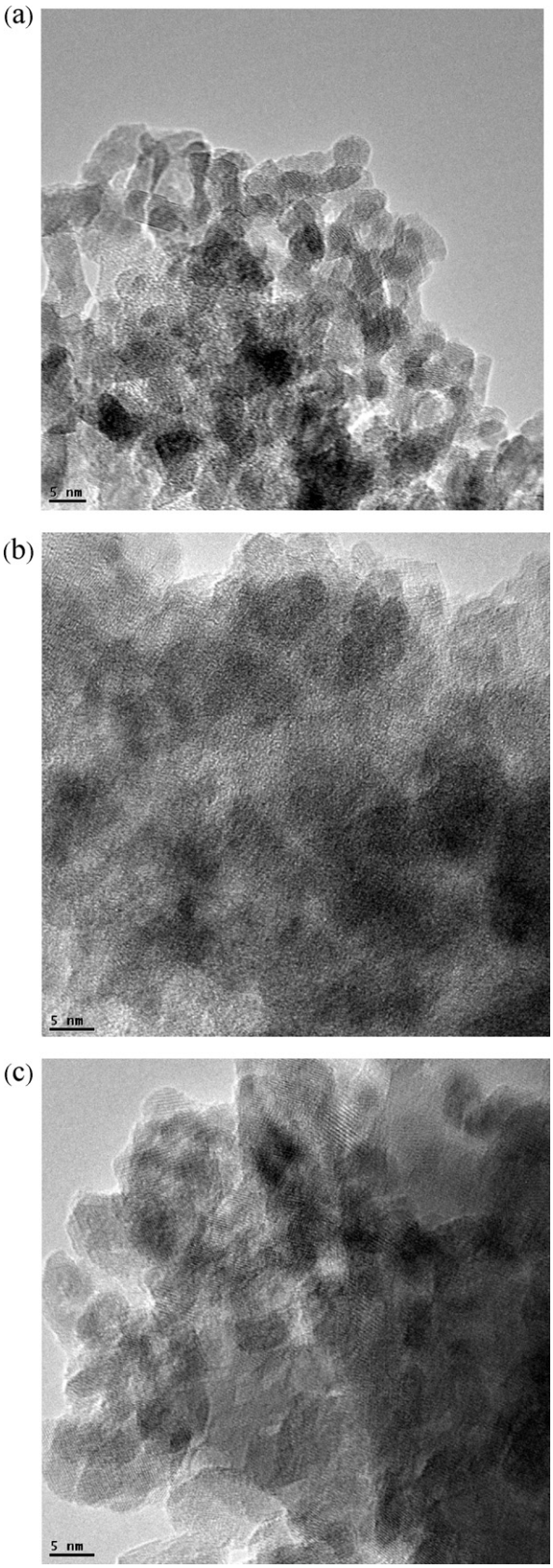

Fig. 3. TEM images of (a) ARM7, (b) TRM7 and (c) RM7.

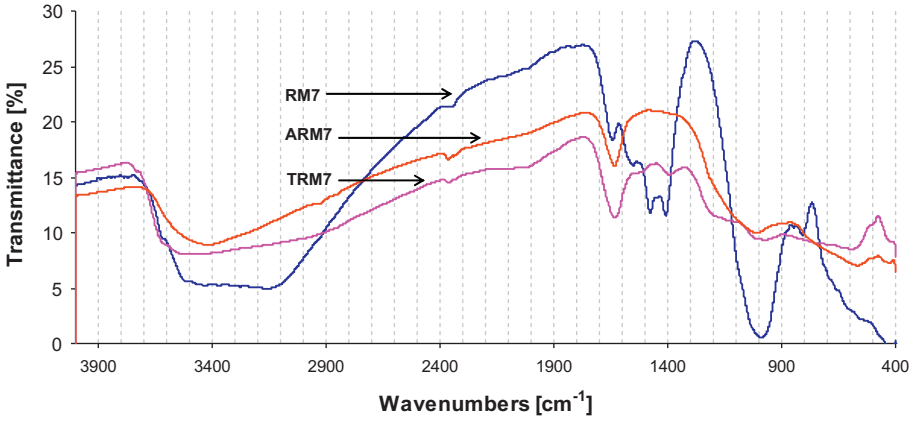

Fig. 4. FTIR spectra of RM7, ARM7 and TRM7.

1632.9 cm^{-1} [27]. A prominent band corresponding to Si—O was detected in RM7 at 989 cm^{-1} and of lower intensities in ARM7 and TRM7 at 1010 cm^{-1} and 970.4 cm^{-1} respectively [27,29].

A typical TPR profile of red mud and α-Fe_2O_3 is similar [30]. It generally consists of two reduction peaks. The first peak represents the conversion of Fe_2O_3 to Fe_3O_4 which occurs around 400 °C, while the second broader peak represents the conversion from $Fe_3O_4 \rightarrow FeO \rightarrow Fe$. The second band may appear around 450–850 °C [30]. The thermal decomposition of goethite to hematite takes place at temperatures >200 °C [12]. However since there is no hydrogen consumption in this step, it is not detected on the TPR profile [31]. In the present study the T_{max} of the first peak for TRM7, ARM7 and RM7 occurred at 418 °C, 449 °C and 462 °C respectively (Fig. 5). The shift to a lower temperature in the T_{max} of the first peak in TRM7 and ARM7 suggests that the reduction of Fe_2O_3 to Fe_3O_4 is easier. The T_{max} of the second peak for ARM7 and TRM7 is observed at 698 °C and 677 °C respectively. In case of RM7 it is around 800 °C. The shift in the peak to a higher temperature in case of RM7 could be due to the decrease in surface area [19] as a result of sintering. In case of TRM7 and ARM7 the sintering agents like Na have been removed by acid treatment consequently resulting in a higher surface area (Table 1). In addition, the presence of hydroxyl group in TRM7 contributes to the shifting of the peak to lower temperature by decreasing the activation energy required for the reduction of hematite to magnetite [32].

3.2. Catalyst activity

Background experiments on the empty reactor showed that below 600 °C there was negligible contribution of the reactor/temperature on CO oxidation. Fig. 6(a) shows the conversion of CO over ARM. Of the three samples, ARM6 shows the best performance while ARM4 shows the lowest conversion. The 50% conversion temperature (*T*50) for ARM6 is 280 °C. The conversion reaches ~90% at 380 °C and complete oxidation is achieved at 420 °C. An isothermal run was also carried out for the ARM samples at 500 °C and the conversion was found to remain >90% throughout the run of 350 min time on stream (Fig. 6(b)).

The performance of TRM was found to be the better than the ARM samples (Fig. 7(a)). The *T*50 temperature for all the samples showed a decrease. The *T*50 temperature for TRM4, TRM6 and TRM7 was 265 °C, 225 °C and 250 °C respectively. TRM6 reached complete oxidation at 340 °C, while both TRM4 and TRM7 reached complete oxidation at 400 °C. The temperature required for TRM4 to reach conversion >90% was 100 °C lower than the ARM.

After the first run for TRM7, the inlet gas flow was stopped and the reactor was allowed to cool in situ. A second cycle was run for

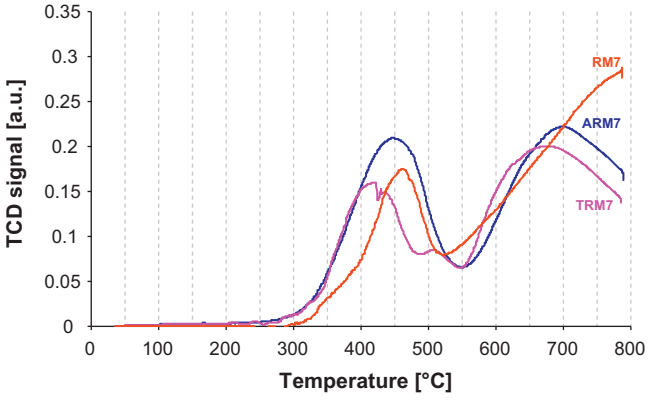

Fig. 5. TPR profile of RM7, ARM7 and TRM7.

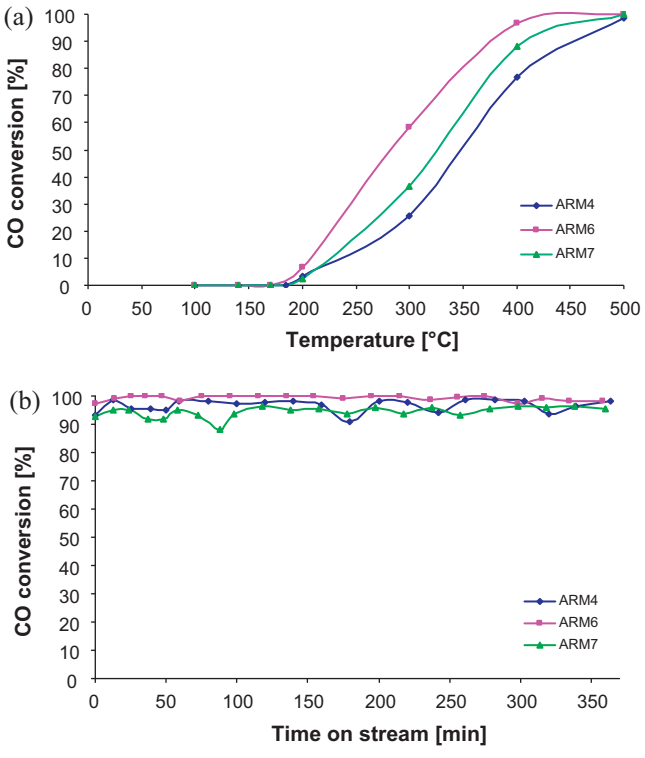

Fig. 6. CO conversion over ARM (1% CO, 6% O_2, GHSV 6000 h^{-1}, 0.5 cm^3 catalyst): (a) temperature programmed run, (b) isothermal run.

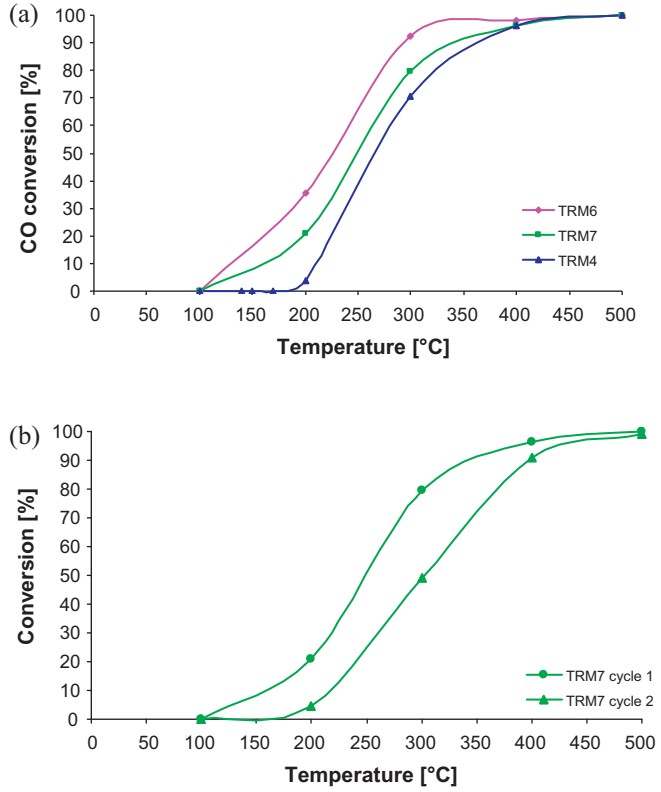

Fig. 7. CO conversion (1% CO, 6% O_2, GHSV 6000 h^{-1}, 0.5 cm^3 catalyst) over (a) TRM, and (b) TRM7 cycles 1 and 2.

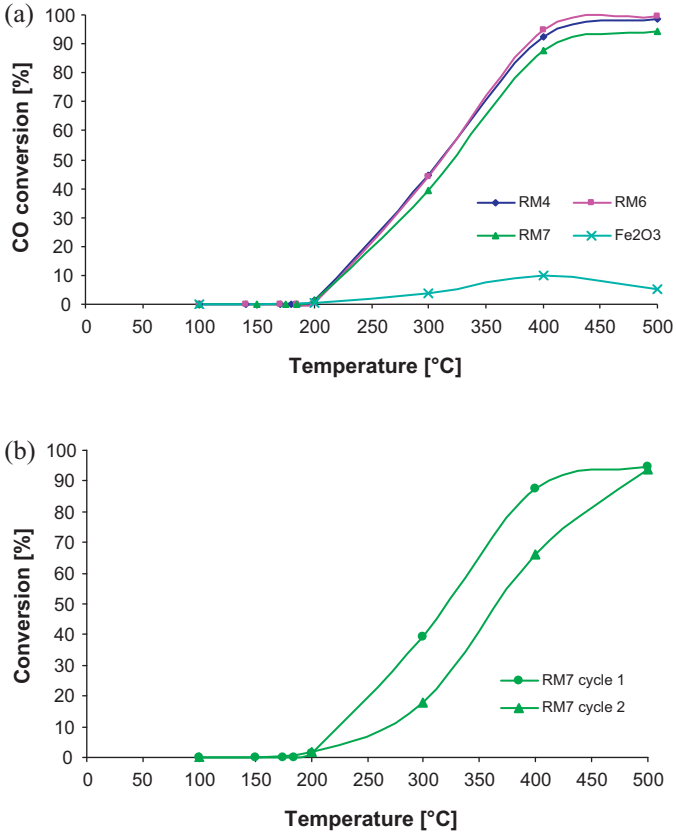

Fig. 8. CO conversion (1% CO, 6% O_2, GHSV 6000 h^{-1}, 0.5 cm^3 catalyst) over (a) RM and Fe_2O_3 powder (b) RM7 cycles 1 and 2.

the same catalyst. A difference of approximately 50 °C was noticed between the *T*50 temperature in cycles 1 and 2. However, at 500 °C TRM7 was able to achieve 94% conversion even in cycle 2 (Fig. 7(b)). The reason for this shift in *T*50 temperature can be attributed to the transformation of the more active hydroxide phases such as goethite (FeO(OH)) into lesser active oxide phases such as hematite (Fe_2O_3) induced by the heating of the sample. According to Reddy et al. [33], CO oxidation takes place following an adsorption mechanism where in the reactants adsorb on the metal oxide surface breaking the O—O bond. The dissociated O atom is picked up by CO forming CO_2. In the two step oxidation mechanism suggested by Mars and Van Krevelen [34], firstly CO is oxidized by the surface oxygen bound to the metal oxide lattice. This creates an oxygen vacancy, and the neighboring metal ion gets reduced to a lower oxidation state. The dioxygen of the gaseous phase then reoxidizes the surface metal atom in the second step. Therefore the ease with which the oxygen atom is released from the metal oxide catalyst is an important factor in determining the activity of the catalyst for CO oxidation. Since the bond length of Fe—O in case of FeO(OH) is longer than in α-Fe_2O_3, it is easier for it to loose the oxygen atom [10]. TGA (thermogravimetry analysis) and ETA (emanation thermal analysis) studies on goethite have shown that there is an increase in micropores in the temperature range 70–310 °C due to loss of water [35]. Above 350 °C the micropores are reduced leading to lowering of surface area. A similar lowering of surface area during the first cycle could also contribute to reduction in activity in the second cycle.

Fig. 8(a) shows the conversion of CO over as-received red mud as a function of temperature in a temperature programmed run. It was found that the *T*50 temperature for all the red mud samples lies within 310–320 °C. The conversion reaches ~90% at 400 °C and complete oxidation is achieved at 500 °C. Similar to the TRM samples the activity of the as-received red mud samples was lower in the second cycle (Fig. 8(b)).

The maximum conversion rate per gram of ARM was calculated for the samples and is summarized in Table 2. The maximum was obtained at 500 °C. The higher rate of reaction in case of ARM and TRM may be attributed to their higher surface area [36]. The rate of reaction calculated by Xu et al. [37], for unsupported nanoporous gold catalyst at room temperature was found to be in the range 2.5×10^{-3} mol g^{-1} h^{-1}–514.8×10^{-3} mol g^{-1} h^{-1} varying with different space velocity.

Fe_2O_3 was also tested under similar conditions for comparison with red mud. It was found that under similar conditions Fe_2O_3 activity remained low and the highest conversion achieved was 9% at 400 °C. This could be attributed to its very low surface area. Moving to higher temperature the activity of Fe_2O_3 dropped further indicating deactivation which may be due to sintering. Similar poor performance has been observed with Fe_2O_3 of 5 μm particle size while iron oxide in the nano form has shown complete conversion at 350 °C [10]. In case of red mud, the activity of iron oxide could

Table 2
Maximum conversion rates.

S. no.	Sample code	Maximum conversion rate (mol g^{-1} h^{-1})
1	RM4	2.7×10^{-3}
2	RM6	2.2×10^{-3}
3	RM7	3.3×10^{-3}
5	TRM4	3.3×10^{-3}
6	TRM6	2.9×10^{-3}
7	TRM7	3.6×10^{-3}
8	ARM4	3.5×10^{-3}
9	ARM6	3.3×10^{-3}
10	ARM7	2.9×10^{-3}

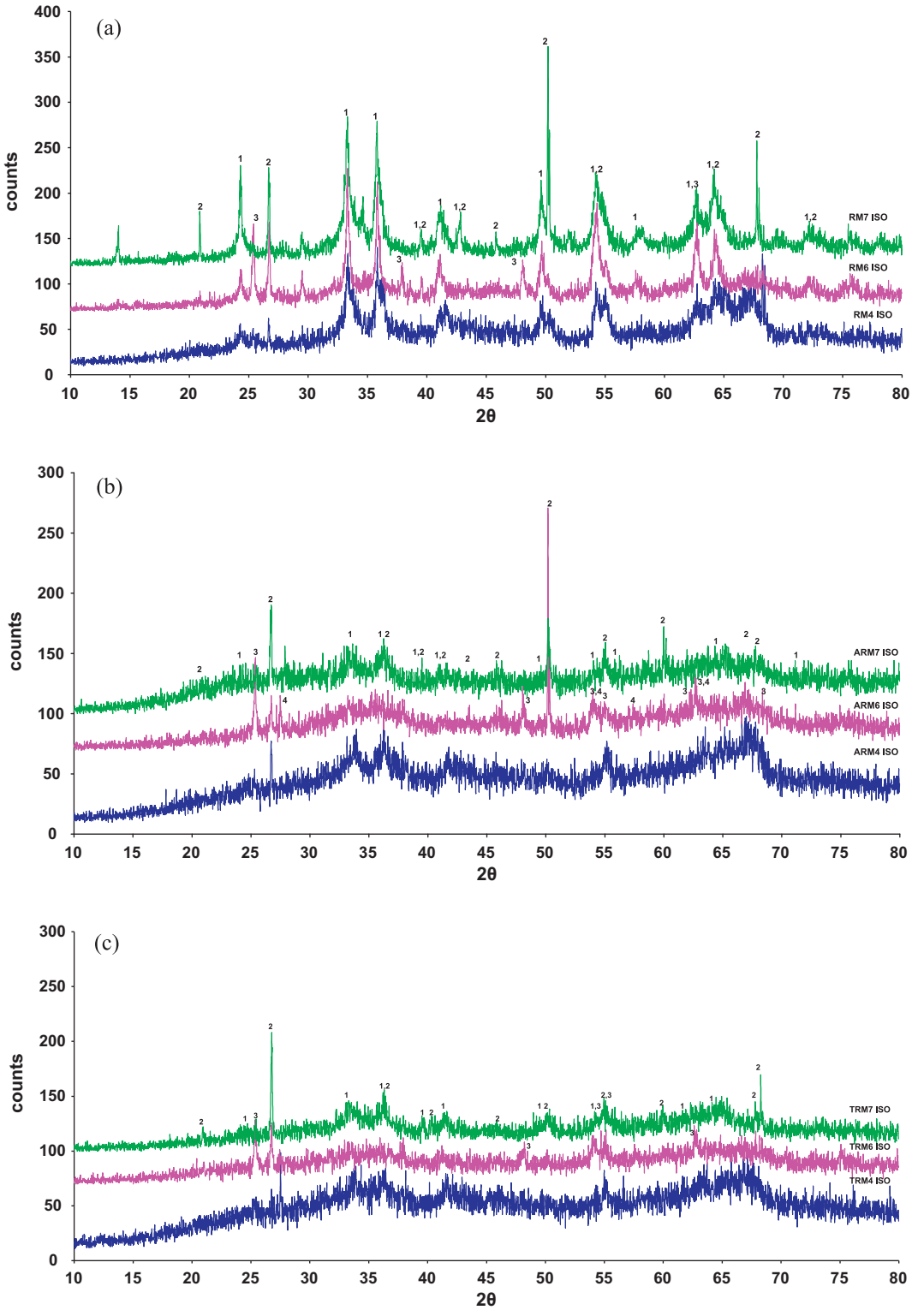

Fig. 9. XRD pattern for post reaction (a) RM, (b) ARM and (c) TRM in an isothermal run. 1: hematite (Fe_2O_3); 2: quartz (SiO_2); 3: anatase (TiO_2); 4: rutile (TiO_2).

have been influenced by the presence of TiO_2, Al_2O_3 and SiO_2. For instance, TiO_2 has been shown to enhance activity of Au catalyst when used as a support for CO oxidation [38].

The higher level of conversion at a lower temperature observed in TRM compared to ARM and RM, corresponds with the TPR data, where TRM showed greater reducibility due to hydroxyl presence. Many studies have investigated influence of iron oxy hydroxides and hydroxide phases in iron oxide based catalysts and supports. TPR studies on iron oxides and hydroxides have shown that presence of OH group facilitates reduction of hematite to magnetite [39–42]. CO oxidation studies on iron oxide/hydroxide catalysts and supports have also observed the same trends [43,44]. Li et al. have observed higher activity of commercial catalyst Nanocat in the first cycle due to the presence of FeOOH phase [10]. Centomo

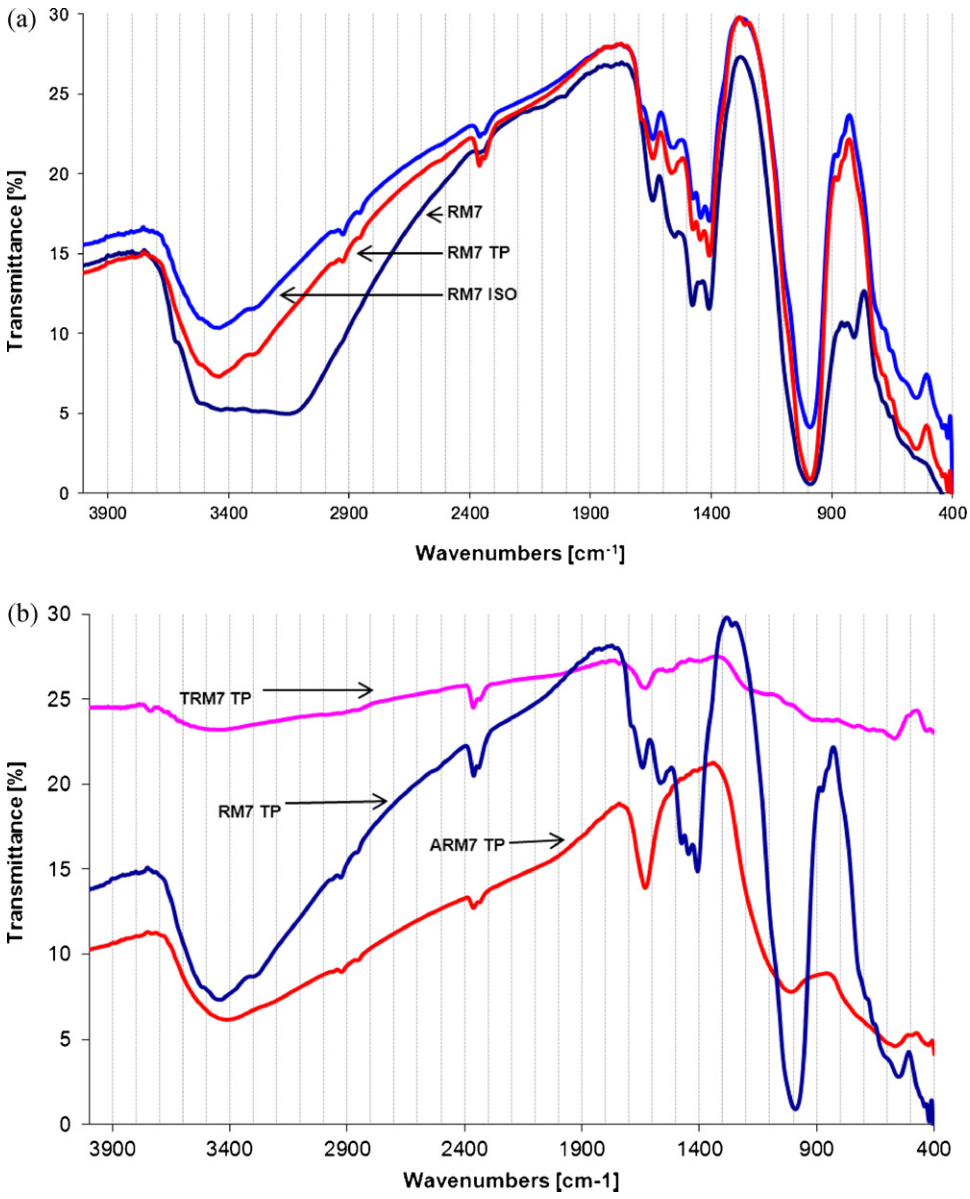

Fig. 10. FTIR pattern for (a) RM7, RM7 TP and RM7 ISO, (b) RM7 TP, TRM7 TP and ARM7 TP.

et al. found that supports with goethite were more active than those with only hematite; however, size of the support also influenced the properties with nanoparticles showing higher activity [45]. Smit et al. attributed the higher activity of OH containing iron catalyst to the formation of HCOO which is then oxidized to CO_2 with lattice oxygen [46].

Fig. 9(a–c) shows the XRD for the post run samples for ARM, TRM and RM respectively from the isothermal run. The patterns for the post reaction samples from the temperature programmed run were similar. It was observed than in all the cases the main phases were hematite and quartz. In case of RM6 anatase could also be seen which was also observed in the pre-reaction sample. The XRD pattern for the post reaction sample showed the transformation of the hydroxide phases into oxide phases due to heating during the reaction in case of RM and TRM. The presence of hematite in the post reaction samples of TRM confirmed the presence of iron hydroxide in the pre-reaction sample in amorphous form.

Fig. 10(a) shows the FTIR spectra of the post-reaction RM7 sample from the isothermal run (RM7-ISO) and the temperature programmed run (RM7-TP) and Fig. 10(b) shows the post reaction RM7, ARM7 and TRM7 from the temperature programmed run. The intensity of the peak relating to OH vibrations had decreased. This decrease was higher in case of the isothermal run due to the exposure of the sample to a higher temperature for a longer duration. It was observed that the peaks relating to goethite near 800 cm^{-1} [28] were no longer present. The Fe–O vibrations relating to hematite could be observed at 549 cm^{-1} and 1642 cm^{-1} in RM7-ISO and at 549 cm^{-1} and 1641 cm^{-1} [27] in RM7 TP. The peak corresponding to the Si–O vibrations was of slightly lower intensity and could be observed at 990 cm^{-1} [27,29] in both RM7 ISO and RM7 TP samples. The post reaction samples of the ARM also showed the presence of hematite and quartz similar to the pre-reaction samples, while the TRM post reaction samples showed only hematite and quartz relating peaks and no goethite, an observation also made in the XRD analysis.

3.3. Apparent activation energy

The apparent activation energy of the reaction was calculated using the Arrhenius plot. Assuming first order reaction [10,47] and

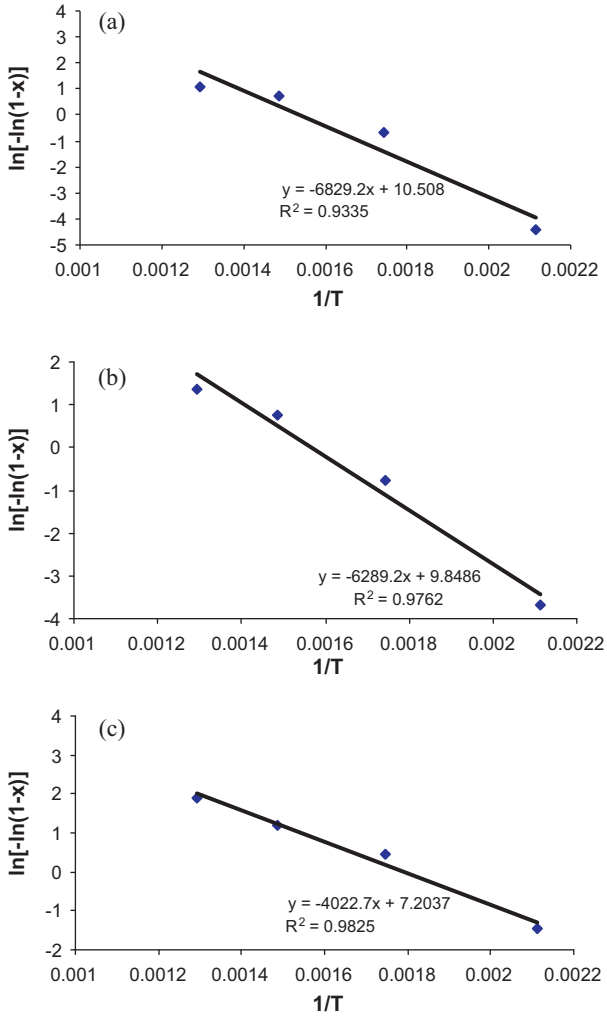

Fig. 11. Apparent activation energy for CO conversion over (a) RM 7, (b) ARM7, (c) TRM7.

substituting the equation for k (Eq. (1)) in Arrehenius equation (Eq. (2)), the following is obtained (Eq. (3)).

$$k = \left(\frac{U}{V}\right) \ln\left(\frac{C_o}{C}\right) \quad (1)$$

$$k = Ae^{-(E/RT)} \quad (2)$$

$$\ln[-\ln(1-x)] = \ln A + \ln\left(\frac{V}{U}\right) - \frac{E}{RT} \quad (3)$$

Here, x is the conversion rate of carbon monoxide to carbon dioxide $x = (C_o - C)/C_o$, U is flow rate (ml s^{-1}), V is volume of catalyst (ml), T is the absolute temperature in Kelvin, R is the gas constant and E_a is the activation energy. $\ln[-\ln(1-x)]$ was plotted versus $1/T$, and the activation energy was calculated from the slope $-E_a/R$ (Fig. 11(a)).

Under the conditions of the reaction with flow rate 50 ml min^{-1} and catalyst weight 400 mg, the activation energy for red mud was calculated to be 13.57 kcal mol^{-1}. The apparent activation energy calculated for ARM7 and TRM7 was 12.49 kcal mol^{-1} and 7.99 kcal mol^{-1} respectively (Fig. 11(b and c)). According to Munteanu et al. [32], the presence of hydroxyl group on the surface reduced the activation energy of the reduction of α-Fe_2O_3 to Fe_3O_4. Li et al. [10] reported the apparent activation energy of iron oxide nanoparticles as 13.5 kcal mol^{-1} with flow rate of 1000 ml min^{-1} and catalyst weight of 50 mg, and for non-nano Fe_2O_3 powder about 20 kcal mol^{-1} [47]. In the present study, low GHSV values were employed. Comparison of activation energies mentioned in the literature must be done with caution since the conditions used in the experiments may be different affecting the final activation energy.

4. Conclusion

Acid treated red muds (TRM and ARM) were found to be more active than the as-received red mud (RM) for CO oxidation. Reducibility at a lower temperature and an increase in surface area was observed in both cases. However the increase in surface area alone cannot explain the increase in activity; the reason for the increase in the activity of the TRM samples was also due to preservation of the hydroxylated iron oxide. Upon drying the precipitated red mud sample at room temperature, large numbers of hydroxylated groups are preserved. The reason for the higher activity of FeOOH over Fe_2O_3 is the relative ease with which it looses the oxygen.

The as-received RM was also shown to be active in CO oxidation. Fe_2O_3 is the main component affecting the catalyzing property of red mud. The presence of hydroxylated phases in cycle 1 make it more active than the subsequent cycles since the breaking of the O—O bond is easier in the former case. The apparent activation energy (E_a) for the reaction for RM was higher than for ARM and TRM. The activity of red mud samples was better than the commercially available red iron oxide.

The paper demonstrates the feasibility of utilizing the waste from the aluminum industry for the oxidation of carbon monoxide.

Acknowledgments

The authors wish to acknowledge Chemistry Department, IITM and Prof. B.S. Rajanikanth, IISc, Bangalore for their help with the TPR analysis. We would also like to acknowledge the help and support extended by the lab staff and colleagues. S.S. gratefully acknowledges the financial support in the form of Senior Research Fellowship provided by CSIR, India.

References

[1] L. Liu, F. Zhou, L. Wang, X. Qi, F. Shi, Y. Deng, Low-temperature CO oxidation over supported Pt, Pd catalysts: particular role of FeO_x support for oxygen supply during reactions, J. Catal. 274 (2010) 1–10.
[2] K. Mallick, M.J. Witcomb, M.S. Scurrell, Simplified single-step synthetic route for the highly active gold-based catalyst for CO oxidation, J. Mol. Catal. A: Chem. 215 (2004) 103–106.
[3] J.N. Lin, B.Z. Wan, Effects of preparation conditions on gold/Y-type zeolite for CO oxidation, Appl. Catal. B 41 (2005) 83–95.
[4] C.Y. Lu, M.Y. Wey, The performance of CNT as catalyst support on CO oxidation at low temperature, Fuel 86 (2007) 1153–1161.
[5] H. Zou, S. Chen, Z. Liu, W. Lin, Selective CO oxidation over CuO—CeO_2 catalysts doped with transition metal oxides, Powder Technol. 207 (2011) 238–244.
[6] X. Liu, J. Liu, Z. Chang, X. Sun, Y. Li, Crystal plane effect of Fe_2O_3 with various morphologies on CO catalytic oxidation, Catal. Commun. 12 (2011) 530–534.
[7] L. Zhang, L. Dong, W. Yu, L. Liu, Y. Deng, B. Liu, H. Wan, F. Gao, K. Sun, L. Dong, Effect of cobalt precursors on the dispersion, reduction, and CO oxidation of CoO_x/(—Al_2O_3 catalysts calcined in N_2, J. Colloid Interface Sci. 355 (2011) 464–471.
[8] P.O. Larsson, A. Andersson, L.R. Wallenberg, B. Svensson, Combustion of CO and toluene: characterization of copper oxide supported on titania and activity comparisons with supported cobalt, iron, and manganese oxide, J. Catal. 163 (1996) 279–293.
[9] M. Shelef, K. Otto, H. Ghandi, The oxidation of CO by O_2 and by NO on supported chromium oxide and other metal oxide catalysts, J. Catal. 12 (1968) 361–375.
[10] P. Li, D.E. Miser, S. Rabiei, R.T. Yadav, M.R. Hajaligol, The removal of carbon monoxide by iron nanoparticles, Appl. Catal. B 43 (2003) 151–162.
[11] K. Mondal, H. Lorethova, E. Hippo, T. Wiltowski, S.B. Lalvani, Reduction of iron oxide in carbon monoxide atmosphere-reaction controlled kinetics, Fuel Process. Technol. 86 (2004) 33–47.
[12] T. Imai, T. Matsui, Y. Fujii, T. Nakai, S.Tanaka, Oxidation catalyst of iron oxide suppressing dioxin formation in polyethylene combustion, J. Mater. Cycles Waste Manag. 3 (2001) 103–109.
[13] J. Yang, B. Xiao, Development of unsintered construction materials from red mud wastes produced in the sintering alumina process, Constr. Build. Mater. 22 (2009) 2299–2307.

[14] S. Wang, H.M. Ang, M.O. Tade, Novel applications of red mud as coagulant, adsorbent and catalyst for environmentally benign processes, Chemosphere 72 (2008) 1621–1635.
[15] G. Power, M. Grafe, C. Klauber, Bauxite residue issues. I. Current management, disposal and storage practices, Hydrometallurgy 108 (2011) 33–45.
[16] C. Klauber, M. Grafe, G. Power, Bauxite residue issues. II. Options for residue utilization, Hydrometallurgy 108 (2011) 11–32.
[17] M. Balakrishnan, V.S. Batra, J.S.J. Hargreaves, A. Monaghan, I.D. Pulford, J.L. Rico, S. Sushil, Catalytic hydrogen production from methane in presence of red mud-making mud magnetic, Green Chem. 11 (2009) 42–47.
[18] S. Sushil, A.M. Alabdulrahman, M. Balakrishnan, V.S. Batra, R. Blackley, J. Clapp, J.S.J. Hargreaves, A. Monaghan, I.D. Pulford, J.L. Rico, W. Zhou, Carbon deposition and phase transformations in red mud on exposure to methane, J. Hazard. Mater. 180 (2010) 409–418.
[19] J.R. Paredes, S. Ordóñez, A. Vega, F.V. Díez, Catalytic combustion of methane over red mud based catalysis, Appl. Catal. B 47 (2004) 37–45.
[20] J.F. Lamonier, F. Wyrwalski, G. Leclercq, A. Aboukaïs, Recyclage d'un déchet, une boue rouge, comme catalyseur pour l'élimination des composés organiques volatils, Can. J. Chem. Eng. 83 (1995) 737–741.
[21] S.E. Khalafalla, L.A. Haas, The role of metallic component in iron–alumina bifunctional catalyst for reduction of SO_2 with CO, J. Catal. 24 (1972) 121–129.
[22] J.F. Lamonier, G. Leclerco, M. Dufour, L. Leclercq, Utilization of red mud. Catalytic properties in selective reduction of nitric oxide by ammonia, Récents Progrès en Génie des Procédés, Boues industrielles: traitements, Valorisation 43 (1995) 31–36.
[23] H. Lin, Y. Chen, W. Wang, Preparation of nanosized iron oxide and its application in low temperature CO oxidation, J. Nanopart. Res. 7 (2005) 249–263.
[24] US Patent 4017425 (1977).
[25] K.C. Pratt, V. Christoverson, Hydrogenation of a model hydrogen-donor system using activated red mud catalyst, Fuel 61 (1982) 460–462.
[26] C.H. Rochester, S.A. Topham, Infrared study of surface hydroxyl groups on haematite, J. Chem. Soc. Faraday Trans. 75 (1979) 1073–1088.
[27] A. Alp, M.S. Goral, Thermal properties of red mud, J. Therm. Anal. Calorim. 73 (2003) 201–207.
[28] R.M. Cornell, U. Schwertmann, The Iron Oxides: Structure, Properties, Reactions, Occurrences and Uses, Wiley-VCH, Germany, 1996.
[29] A. Gök, M. Omastováa, J. Prokeš, Synthesis and characterization of red mud polyaniline composites: electrical properties and thermal stability, Eur. Polym. J. 43 (2007) 2471–2480.
[30] S. Ordóñez, H. Sastre, F.V. Díez, Characterisation and deactivation studies of sulphided red mud used as catalyst for the hydrodechlorination of tetrachloroethylene, Appl. Catal. B 29 (2001) 263–273.
[31] B.C. Campo, O. Rosseler, M. Alvarez, E.H. Rueda, M.A. Volpe, On the nature of goethite, Mn–goethite and Co–goethite as supports for gold nanoparticles, Mater. Chem. Phys. 109 (2008) 448–454.
[32] G. Munteanu, L. Ilieva, D. Andreeva, Kinetic parameters obtained from TPR data for α-Fe_2O_3 and Au/α-Fe_2O_3 systems, Thermochim. Acta 291 (1997) 171–177.
[33] B.V. Reddy, F. Rasouli, M.R. Hajaligol, S.N. Khanna, Novel mechanism for oxidation of CO by Fe_2O_3 clusters, Fuel 83 (2004) 1537–1541.
[34] P. Mars, V. Krevelen, Oxidations carried out by means of vanadium oxide catalysts, Chem. Eng. Sci. 3 (1954) 41–59.
[35] V.Balek, J. Subrt, Thermal behaviour of iron (1 1 1) oxide hydroxides, Pure Appl. Chem. 67 (1995) 1839–1842.
[36] US Patent 3,992,327 (1976).
[37] C. Xu, X. Xu, J. Su, Y. Ding, Research on unsupported nanoporous gold catalyst for CO oxidation, J. Catal. 252 (2007) 243–248.
[38] K. Fukushima, G.H. Takaoka, J. Matsuo, I. Yamada, Effects on CO oxidation activity of nano-scale Au islands and TiO_2 support prepared by the ionized cluster beam method, Jpn. J. Appl. Phys. 36 (1997) 813–818.
[39] G. Munteanu, L. Ilieva, D. Andreev, Kinetic parameters obtained from TPR data for α-Fe_2O_3 and Au/α-Fe_2O_3 systems, Thermochim. Acta 291 (1997) 171–177.
[40] L.I. Iheva, D.H. Andreev, A.A. Andreev, TPR and TPD investigation of Au/α-Fe_2O_3, Thermochim. Acta 292 (1997) 169–174.
[41] G. Neri, A.M. Visco, S. Galvagno, A. Donato, M. Panzalorto, Au/iron oxide catalysts: temperature programmed reduction and X-ray diffraction characterization, Thermochim. Acta 329 (1999) 39–46.
[42] C. Milone, R. Ingoglia, L. Schipilliti, C. Crisafulli, G. Neri, S. Galvagno, Selective hydrogenation of α,β-unsaturated ketone to α,β-unsaturated alcohol on gold-supported iron oxide catalysts: role of the support, J. Catal. 236 (2005) 80–90.
[43] B. Qiao, Y. Deng, Highly effective ferric hydroxide supported gold catalyst for selective oxidation of CO in the presence of H_2, Chem. Commun. 17 (2003) 2192–2193.
[44] B. Qiao, L. Liua, J. Zhang, Y. Deng, Preparation of highly effective ferric hydroxide supported noble metal catalysts for CO oxidations: from gold to palladium, J. Catal. 261 (2009) 241–244.
[45] P. Centomo, M. Zecca, V.D. Noto, S. Lavina, G.G. Bombi, L. Nodari, G. Salviulo, R. Ingoglia, C. Milone, S. Galvagno, B. Corain, Characterization of synthetic iron oxides and their performance as support for Au catalysts, ChemCatChem 2 (2010) 1143–1149.
[46] G. Smit, S. Zrncevic, K. Lazar, Adsorption and low-temperature oxidation of CO over iron oxides, J. Mol. Catal. A: Chem. 252 (2006) 103–106.
[47] J.S. Walker, G.I. Straguzzi, W.H. Manogue, G.C.A. Schuit, Carbon monoxide and propene oxidation by iron oxides for auto-emission control, J. Catal. 2 (1998) 298–309.